

Structural and Magnetic Properties of Monophasic Maghemite (γ -Fe₂O₃) Nanocrystalline Powder

Juan Adrián Ramos Guivar^{1*}, Arturo Isaías Martínez², Ana Osorio Anaya³, Luis De Los Santos Valladares⁴, Lizbet León Félix⁵, Angel Bustamante Dominguez¹

¹Laboratorio de Cerámicos y Nanomateriales, Facultad de Ciencias Físicas, Universidad Nacional Mayor de San Marcos, Lima, Perú

²Centro de Investigación y Estudios Avanzados del Instituto Politécnico Nacional, Cinvestav, Unidad Saltillo, Ciudad de México, México

³Laboratorio de Nanotecnología e Innovación Tecnológica, Departamento de Química e Ingeniería Química, Universidad Nacional Mayor de San Marcos, Lima, Perú

⁴Cavendish Laboratory, Department of Physics, University of Cambridge, Cambridge, UK

⁵Núcleo de Física Aplicada, Instituto de Física, Universidade de Brasília, Brasília, Brasil

Email: *aguivar@gmail.com, angelbd1@gmail.com

Received 10 May 2014; revised 22 June 2014; accepted 9 July 2014

Copyright © 2014 by authors and Scientific Research Publishing Inc.

This work is licensed under the Creative Commons Attribution International License (CC BY).

<http://creativecommons.org/licenses/by/4.0/>



Open Access

Abstract

Structural and magnetic studies of monophasic maghemite (γ -Fe₂O₃) magnetic nanocrystallites (MNCs) synthesized by the co-precipitation chemical route are reported in this paper. For the synthesis, a starting precursor of magnetite (Fe₃O₄) in basic medium was oxidized at room temperature by adjusting the pH = 3.5 at 80°C in an acidic medium without surfactants. X-ray diffraction (XRD) pattern shows widened peaks indicating nanometric size and Rietveld Refinement confirms only one single-phase assigned to γ -Fe₂O₃ MNCs. High Resolution Transmission Electron Microscopy (HR-TEM) demonstrates the formation of nanoparticles with diameter around $D \approx 6.8 \pm 0.1$ nm which is in good agreement with Rietveld Refinement (6.4 ± 1 nm). A selected area electron diffraction pattern was carried out to complement the study of the crystalline structure of the γ -Fe₂O₃ MNCs. $M(H)$ measurements taken at different temperatures show almost zero coercivity and remanence indicating superparamagnetic domain and high magnetic saturation.

Keywords

Monophasic Nanomaghemite, Rietveld Refinement, TEM, SAED, M - H Loops, ZFC

*Corresponding author.

1. Introduction

In recent years, super paramagnetic iron oxides nanoparticles (SPIONS) such as magnetite (Fe_3O_4) and maghemite ($\gamma\text{-Fe}_2\text{O}_3$) have attracted different areas of technology. Some of them include antitumor drug delivery [1], removal of industrial pollutants from water [2], manipulation of biomedical objects [3].

In addition, they can be applied in solid-state-phase absorbents of human genomic DNA [4], green catalysts [5], thin film from protection corrosion [6], gas sensors [7], magnetic resonance imaging (MRI) contrast optimization [8] and hyperthermia treatment [9]. In the case of maghemite nanoparticles, their surface can be modified (functionalization) and mechanically controlled by an external magnetic field, therefore they are promising in medicine such as drug deliverers for cancer therapy [10].

Up to date, many reports have described different methods to synthesize magnetite and maghemite MNCs. Some of them include electrochemical method [11], laser pyrolysis [12], microemulsion synthesis [13], and hydrothermal technique [14]. In this work, we report the preparation of $\gamma\text{-Fe}_2\text{O}_3$ nanocrystallites by co-precipitation chemical procedure. This method is chosen because of the lower temperatures required to the synthesis compared to other techniques such as hydrothermal technique [14] which require interval of temperature from 130°C to 250°C and high vapor pressure (from 0.3 to 4 MPa). On the other hand, in our previous report [15], we studied the intermediate super paramagnetic relaxation effect of $\gamma\text{-Fe}_2\text{O}_3$ nanoparticles by Mössbauer spectroscopy at different temperatures. The relaxation process was broken by decreasing the temperature up to 4.2 K proving the single-phase formation of the MNCs fitting the spectrum with the corresponding two typical hyperfine fields of maghemite. In this work we characterize the obtained nanocrystallites by transmission electron microscopy (TEM), selected area electron diffraction (SAED) and X-ray diffraction (XRD) to confirm the purity and the formation of monophasic $\gamma\text{-Fe}_2\text{O}_3$ MNCs. Besides, for a more accurate calculation of the blocking temperature and the magnetic diameter, in this work we perform the magnetic measurements at different temperatures.

2. Experimental

Homogeneous maghemite $\gamma\text{-Fe}_2\text{O}_3$ MNCs were obtained by the coprecipitation technique following the next procedure. Initially, magnetite (Fe_3O_4) nanoparticles precursor were prepared from ferric chloride and ferrous chloride with stoichiometric ratio of $\text{Fe}^{2+}/\text{Fe}^{3+}$ (1:2) in aqueous solution (basic medium of $\text{pH} = 11 - 12$) without surfactants or organic solvents. 0.85 mL of 12.1 N HCl and 25 mL of deoxygenated water were added.

Besides, 5.2 g of FeCl_3 and 2.0 g of FeCl_2 were dissolved in the solution under continuous stirring. The resulting solution was dropped wise into 250 mL of 1.5 M NaOH solution under vigorous stirring up to obtain a black precipitate with $\text{pH} = 12$. The paramagnetism was checked in situ by placing a magnet near the system. Purified deoxygenated water was added to the precipitate and this solution was decanted by centrifugation at 4000 rpm. After repeating the last procedures three times, 500 mL of 0.01 M HCl solution was added to the precipitate with stirring in order to neutralize the anionic charges on the nanoparticles. Immediately, the oxidation of Fe_3O_4 into $\gamma\text{-Fe}_2\text{O}_3$ was carried out by adjusting the $\text{pH} = 3.5$ with hydrochloric acid. The oxidation was controlled under magnetic stirring at about 80°C for 30 min to get maghemite phase. The sample was dried at about 40°C with the aim of getting a reddish-brown color, which is characteristic from maghemite MNCs [16]. The characterization was done by X-ray Diffraction (XRD) in a Bruker D8 equipment with radiation $K_{\alpha 1}$ of copper ($\lambda = 1.54056 \text{ \AA}$) in the range from 8 to 80 degrees, with a step of 0.02 degrees, at room temperature (RT). The X-ray diffraction pattern was analyzed by the Rietveld Refinement method using the DBWS program, the peaks shape was modeled with a Pseudo-Voigt function and the crystallite size is related to the line width (Γ) that was estimated with the use of the Scherrer formula. For TEM measurements, we have used the Titan 80 - 300 kV microscope equipped with a special high-brightness Schottky-field emission electron source. We have used the Gauss program, developed at the Cadiz University, Spain, for counting nanoparticles with spherical shape. Measurements of the magnetic moment as a function of applied fields were carried out in a DC MPMS-SQUID magnetometer (Quantum Design) in a range of -55 k Oe to 55 k Oe at different temperatures from 10 K to 300 K. Measurements of the magnetic moment as a function of the temperature in the range 10 - 300 K were carried out by applying three different magnetic fields in zero field cooling (ZFC) mode.

3. Results and Discussions

The XRD pattern of the sample is shown in **Figure 1**. It reveals a monophasic sample with wide peaks due to

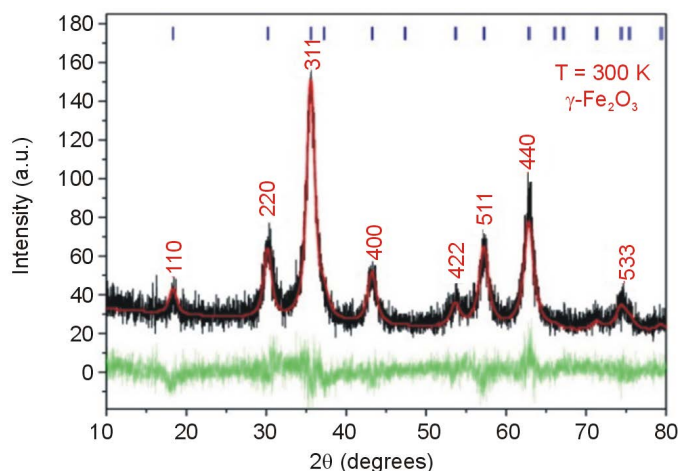


Figure 1. Rietveld Refinement of the XRD pattern of the maghemite MNCs obtained by co-precipitation. The black line corresponds to the experimental data, the red line is the theoretical diffractogram obtained after several refinements and the green line is the difference between the experimental and theoretical data. The Miller indexes are indicated in the top by the blue lines, and they are fully written in the strongest peaks.

the nanometric size of the crystallites. The diffractogram fits very well with the cubic symmetry (space group $P4_132$) of $\gamma\text{-Fe}_2\text{O}_3$ (PDF Card 39-1346).

Rietveld Refinement was performed which give a mean grain diameter of 6.4 ± 1 nm. The value of the uncertainty can be associated to the noisy background of the diffractogram commonly obtained in iron oxide magnetic nanoparticles [17].

Table 1 summarizes the refined parameters obtained for maghemite structure. We observed from the Rietveld analysis the single phase of maghemite formed without any impurities. In addition, the obtained lattice parameters $a = b = c = 8.3565$ (Å) confirm the presence of the cubic structure and good crystallinity obtained during the chemical reaction.

Notably, the interplanar distance corresponding to $2\theta = 43.284^\circ$ is $d_{(400)} = 2.082$ Å which is similar to the value reported by Hai *et al.* [18]. This value is helpful to differentiate between the XRD pattern of the maghemite ($d_{(400)} = 2.0886$ Å, $2\theta = 43.28^\circ$) and magnetite ($d_{(400)} = 2.0993$ Å, $2\theta = 43.052^\circ$) phases due to the shift at 2θ value. **Figure 2(a)** shows the bright TEM image of the maghemite MNCs. The sample consists on agglomerated particles with nearly spherical shape and diameter ranging from 6 to 10 nm.

The agglomeration could be prevented by using oleic acid [19] [20]. The top left inset of this figure shows the selected area electron diffraction (SAED) pattern indexed with the cubic structure of the maghemite phase (JCPDS No. 39-1346). Note the presence of the plane reflection (400) remarked in the XRD above. The size distribution is presented in the bottom right inset of the figure. A mean diameter size of $D = 6.8 \pm 0.1$ nm is calculated which is close to that obtained by Rietveld Refinement above (6.4 ± 1 nm). **Figure 2(b)** shows a high resolution (HR) TEM image. The degree of agglomeration, size, round shape and grain bordering are better distinguished in this figure. Remarkably, the cubic structure of the maghemite phase obtained by the XRD above is confirmed by the fast Fourier transform (FFT) image which is shown in the top right inset of **Figure 2(b)** and revealing the (111), (220), (311) and (400) Miller indexes. The texture of the crystallites is better appreciated in the top left inset on this figure. The (111) indexes correspond to planes separated with $d = 4.8$ Å, whereas the (220) indexes to planes separated with $d = 2.9$ Å confirming the XRD analysis.

Table 2 summarizes and compares the values of these interplanar distances obtained by the XRD and HRTEM measurements. The corresponding FFT image of the zoomed area is also shown in the bottom left inset of the figure.

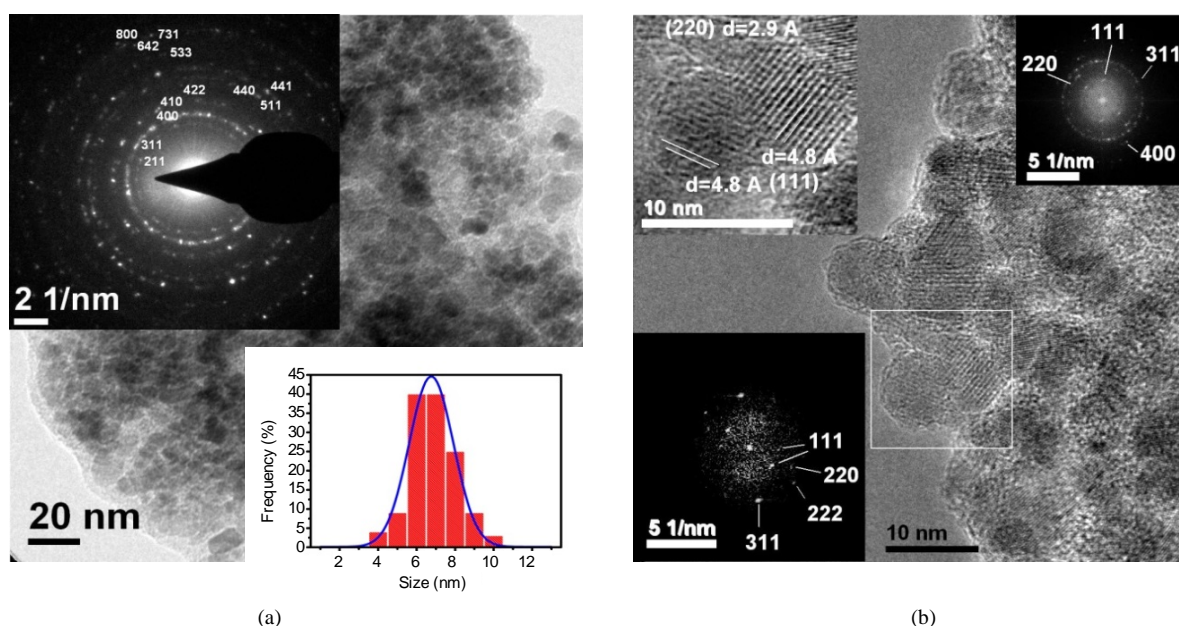
The magnetization dependence on magnetic field (M - H) loops of the maghemite MNCs measured at different temperatures are shown in **Figure 3**. The curves were fitted with the law of approach for high magnetic regions to estimate the saturation magnetization (M_s) values [21]:

Table 1. Refined structural parameters for the γ -Fe₂O₃ phase, ($R_{WP}/R_{exp} = 1.12$).

| Atom | Wyckoff | x/a | y/b | z/c | Occupancy |
|---------------------------|---------|--------------------------|---------|---------|-----------|
| Fe (1) | 8b | 1/2 | 1/2 | 1/2 | 0.04167 |
| Fe (2) | 16c | 1/8 | 1/8 | 1/8 | 0.08333 |
| O | 32e | 0.25741 | 0.25741 | 0.25741 | 0.16667 |
| Lattice parameters | | $a = b = c = 8.3565$ (Å) | | | |

Table 2. Corresponding interplanar distances for the diffraction peaks (111) and (220) of maghemite MNCs obtained by XRD and HR-TEM techniques.

| Peak of diffraction | Interplanar distance obtained by XRD (in Å) | Interplanar distance obtained by TEM (in Å) |
|---------------------|---|---|
| 111 | 4.8 | 4.8 |
| 220 | 2.9 | 2.9 |

**Figure 2.** TEM analysis of maghemite MNCs. (a) Bright TEM: The insets show the indexed SAED pattern and the mean diameter value obtained by fitting the size distribution with a Gaussian function was $D = 6.8 \pm 0.07$ nm; (b) HR-TEM: The top right inset shows the FFT image of the complete area, the top left inset shows a zoom image of an area revealing the crystalline planes and the bottom left inset shows the respective FFT image of this zoomed area.

$$M = M_s \times \left(1 - \frac{a}{H} - \frac{b}{H^2} \right) + \chi \times H \quad (1)$$

where the term $\chi \times H$ represents the field-induced increase in the spontaneous magnetization of the magnetic domains, or forced magnetization. This term is really small at temperatures below the Curie transition point (T_c), thus it may be neglected. Importantly, Equation (1) is used just for values of temperatures below T_c . Besides, a and b are important parameters associated to the theoretical physics phenomena; a is related to inclusions and/or microstress, and b is related to crystal anisotropy [22].

Where K_{eff} is the effective magnetic anisotropy and M_s is the saturation magnetization. **Figure 4(a)** and **Figure 4(b)** show the best fitting of Equation (1) to the experimental data of the M - H loops for $T = 10$ K and 300 K. **Figure 4(c)** shows the behavior of the saturation magnetization with the temperature. At RT the value of M_s is near to that reported for bulk maghemite (60 emu/g) [23]. This indicates that eventual chemical residuals or dead layers formed on the surfaces of the MNCs [18] during the nucleation process are of minor influence proving a

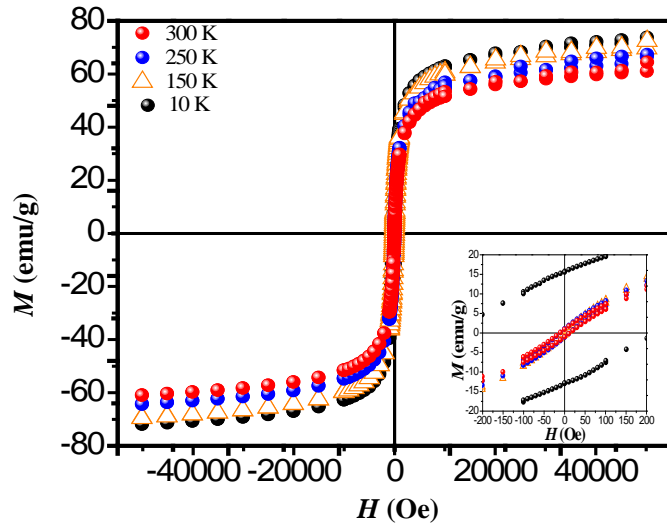


Figure 3. M - H loops measured at different temperatures 10, 150, 250 and 300 K and under applied magnetic fields between $-55,000$ to $55,000$ Oe. The inset shows the zoom plot of hysteresis loops obtained at different temperatures. We can regard the thermal dependence of the coercive field, which suggested the presence of superparamagnetism state at RT.

high degree of purity of our sample as also confirmed with Rietveld Refinement and SAED patterns. Besides, the fitting of the thermal dependence of the coercive field (in the top right inset of **Figure 4(d)**) shows a behavior as a function of squared root of T for temperatures below $T < 50$ K which could be associated to low interparticle interactions [24]. Hence the fitting yields a mean value for the blocking temperature $\langle T_B \rangle = 62 \pm 3$ K. Note that there is a slight increment in the coercive field above 150 K. This unexpected behavior was also reported in other systems such as CoFe_2O_4 nanoparticles and can be associated with rotation of the magnetic moments from coherent to incoherent modes [24]. The mean blocking temperature can be also calculated from the ZFC signals (**Figure 5(a)**), assuming grains with the same diameter and following the relation:

$$\langle T_B \rangle = T_{\max} / \beta \quad (2)$$

with $1.5 < \beta < 2$ [25]. Taking a value of $\beta = 1.6$ and considering that $T_{\max} = 105 \pm 3$ K (which is obtained from the curve with applied magnetic field of 500 Oe), we obtain $\langle T_B \rangle = 66 \pm 3$ K.

This value is in good agreement with the one determined from the temperature dependence of the coercive field above. Note that in the **Figure 5(b)** T_{\max} tends to shift to lower values when the applied magnetic field is increased [25]. The effective magnetic anisotropy is given by $K_{\text{eff}} = \frac{25K_B T_B}{V}$, where k_B is the Boltzmann constant ($1.38 \times 10^{-23} \text{ J} \cdot \text{K}^{-1}$) and $\langle V \rangle$ is the mean volume of the particles. Thus, $K_{\text{eff}} = 1.6 \times 10^4 \text{ J/m}^3$. Both values for K_{eff} obtained by the fit of the thermal coercive field and the ZFC relations at 500 and 100 Oe are similar. Nevertheless, these values are higher than that for bulk maghemite ($4.7 \times 10^3 \text{ J/m}^3$). This is because in the nano-scale, K_{eff} varies with size as $1/D$ [26].

The magnetic diameter is calculated with the formula [27]:

$$D_{\text{MAG}} = \left[\frac{18K_B T}{\pi} \frac{\chi_i}{\rho M_S^2} \right]^{1/3} \quad (3)$$

where $\chi_i = \left(\frac{dM}{dH} \right)_{H \rightarrow 0}$ is an initial susceptibility of the system, k_B is again the Boltzmann constant, M_S is the

saturation magnetization calculated for $T = 300$ K (60 emu/g), and ρ is the density of the maghemite ($4.87 \frac{\text{g}}{\text{cm}^3}$).

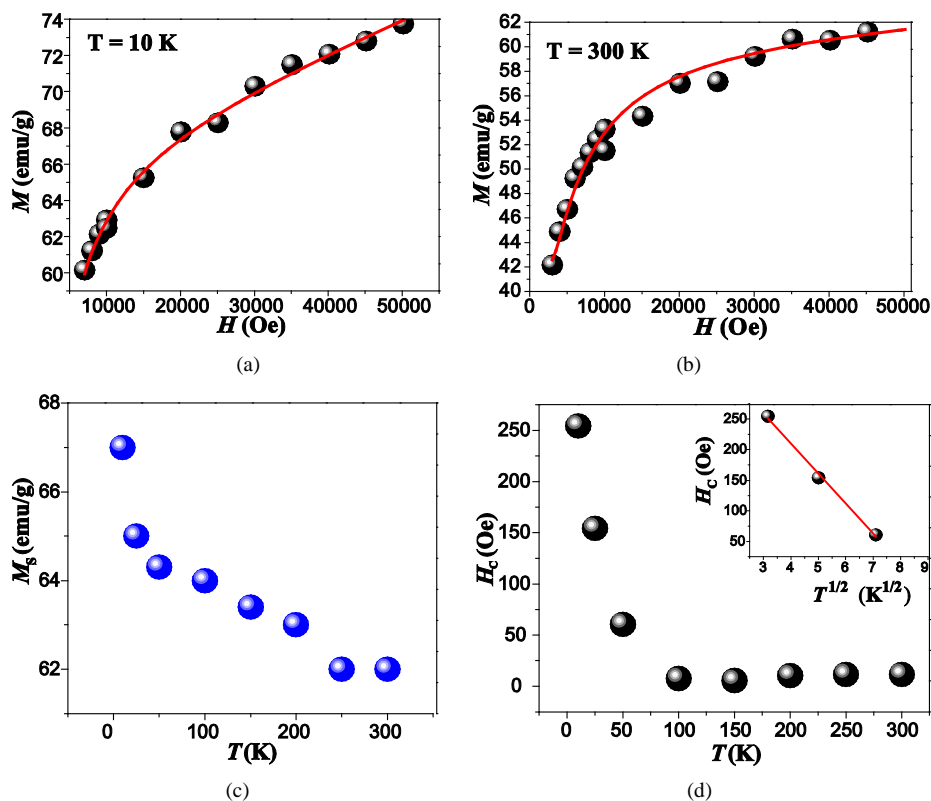


Figure 4. Fitting of the M - H loop obtained at 10 K (a) and at 300 K (b), dependence of M_S vs T (c) and temperature dependence of the coercive field (d) for maghemite MNCs obtained by co-precipitation. (The inset in (d) shows the fitting for the lowest temperatures).

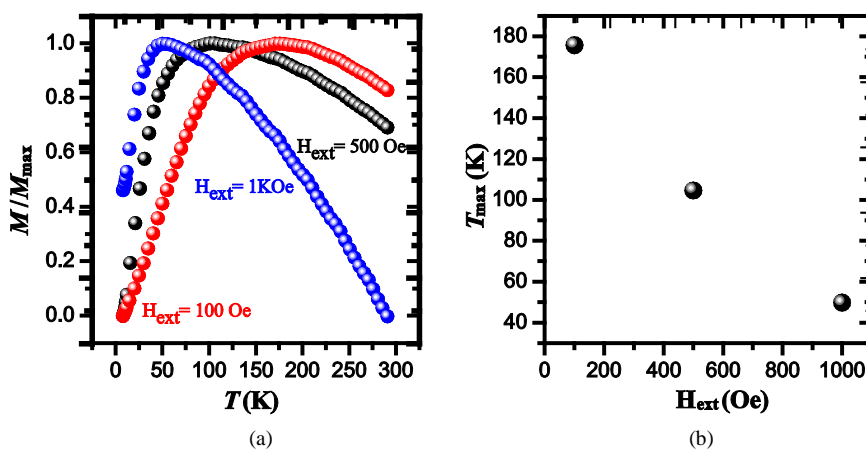


Figure 5. Normalized ZFC magnetization curves obtained under $H_{ext} = 100$ Oe, 500 Oe and 1 kOe (a) and T_{max} dependence with the applied magnetic field (b) for maghemite nanoparticles prepared by co-precipitation.

An initial susceptibility obtained from M - H loop at 300 K (**Figure 4(b)**) is 0.02 emu/g Oe, yielding to a value of $D_{MAG} = 6.5$ nm which is in good agreement with the mean values obtained by XRD and TEM analysis.

4. Conclusions

Magnetite with molar ratio Fe^{2+}/Fe^{3+} 1:2 was oxidized to form maghemite MNCs by following the co-precipitation method. The average sizes of the particles estimated by Rietveld Refinement and HRTEM are 6.4 ± 1 and

6.8 ± 0.1 nm, respectively. The average size of the magnetic domains calculated from the magnetic measurements is 6.5 nm, confirming that the maghemite MNCs are constituted of single magnetic domains. Good crystallinity and single-phase formation are discussed and confirmed in detail by XRD (Rietveld analysis), TEM and SAED analysis. Additionally, coercive thermal dependence and $M(T)$ measurements yield valuable and reliable information about the mean blocking temperature ($\langle T_B \rangle = 62 \pm 3$ K and $\langle T_B \rangle = 66 \pm 3$ K, respectively). The magnetocrystalline anisotropy constant is $K_{\text{eff}} = 1.6 \times 10^4$ J/m³ respectively. High magnetic saturation is obtained showing that not chemical residuals on the surface of the MNCs are formed during the chemical reaction, confirming once again the monophasic formation of MNCs. Therefore, co-precipitation is a reliable technique to synthesize homogeneous and pure maghemite nanoparticles.

Acknowledgements

The work in Cambridge has been supported by the Engineering and Physical Science Research Council (EPSRC).

References

- [1] Yu, S.F., Wu, G.L., Gu, X., Wang, J.J., Wang, Y.N., Gao, H. and Ma, J.B. (2013) Magnetic and pH-Sensitive Nanoparticles for Antitumor Drug Delivery. *Colloids and Surfaces B: Biointerfaces*, **103**, 15-22. <http://dx.doi.org/10.1016/j.colsurfb.2012.10.041>
- [2] Asuha, S., Gao, Y.W., Deligeer, W., Yu, M., Suyala, B. and Zhao, S. (2011) Adsorptive Removal of Methyl Orange Using Mesoporous maghemite. *Journal of Porous Materials*, **18**, 581-587. <http://dx.doi.org/10.1007/s10934-010-9412-2>
- [3] Liu, Y., Gao, Y. and Xu, C.J. (2013) Using Magnetic Nanoparticles to Manipulate Biological Objects. *Chinese Physics B*, **22**, Article ID: 097503.
- [4] Shan, Z., Wu, Z., Chen, H., Zhang, Z.M., Zhou, Y., Wen, A.X., Oakes, K.D. and Servos, M.R. (2012) PCR-Ready Human DNA Extraction from Urine Samples Using Magnetic Nanoparticles. *Journal of Chromatography B*, **881-882**, 63-68.
- [5] Zare, L. and Nikpassand, M. (2012) Evaluation of Nano Fe₃O₄ as a Green Catalyst for the Synthesis of Mono, Bis and Tris Diindolyl Methanes. *Journal of Chemistry*, **9**, 1623-1631.
- [6] Chandrappa, K.G. and Venkatesha, T.V. (2012) Electrochemical Bulk Synthesis of Fe₃O₄ and α -Fe₂O₃ Nanoparticles and Its Zn-Co- α -Fe₂O₃ Composite Thin Films for Corrosion Protection. *Materials and Corrosion*, **63**, Article No. 9999.
- [7] Zhang, S.F., Ren, F., Wu, W., Zhou, J., Xiao, X.H., Sun, L.L., Liu, Y. and Jiang, C.Z. (2013) Controllable Synthesis of Recyclable Core Shell γ -Fe₂O₃:SnO₂ Hollow Nanoparticles with Enhanced Photocatalytic and Gas Sensing Properties. *Physical Chemistry Chemical Physics*, **15**, 8228. <http://dx.doi.org/10.1039/c3cp50925g>
- [8] Zhang, S., Qi, Y.Y., Yang, H., Gong, M.F., Zhang, D. and Zou, L.G. (2013) Optimization of the Composition of Bi-metallic Core/Shell Fe₂O₃/Au Nanoparticles for MRI/CT Dual-Mode Imaging. *Journal of Nanoparticle Research*, **15**, 2023.
- [9] Lee, S.-C., Fu, C.-M. and Chang, F.-H. (2013) Effects of Core/Shell Structure on Magnetic Induction Heating Promotion in Fe₃O₄/ γ -Fe₂O₃ Magnetic Nanoparticles for Hyperthermia. *Applied Physics Letters*, **103**, Article ID: 163104. <http://dx.doi.org/10.1063/1.4825270>
- [10] Verma, N.K., Crosbie-Staunton, K., Satti, A., Gallagher, S., Ryan, K.B., Doody, T., McAtamney, C., MacLoughlin, R., Galvin, P., Burke, C.S., Volkov, Y. and Gun'ko, Y.K. (2013) Magnetic Core-Shell Nanoparticles for Drug Delivery by Nebulization. *Journal of Nanobiotechnology*, **11**, 1. <http://dx.doi.org/10.1186/1477-3155-11-1>
- [11] Fajaroh, F., Setyawan, H., Nur, A. and Wuled Lenggoro, I. (2013) Thermal Stability of Silica-Coated Magnetite Nanoparticles Prepared by an Electrochemical Method. *Advanced Powder Technology*, **24**, 507-511. <http://dx.doi.org/10.1016/j.apt.2012.09.008>
- [12] Moussa, S., Atkinson, G. and Samy El-Shall, M. (2013) Laser-Assisted Synthesis of Magnetic Fe/ Fe₂O₃ Core: Carbon-Shell Nanoparticles in Organic Solvents. *Journal of Nanoparticle Research*, **15**, 1470.
- [13] Podrepsek, G.H. and Leitgeb, Z.K.M. (2013) Different Preparation Methods and Characterization of Magnetic Coated with Chitosan. *Journal of Nanoparticle Research*, **15**, 1751. <http://dx.doi.org/10.1007/s11051-013-1751-x>
- [14] Liu, Q.C., Zi, Z.F., Zhang, M., Pang, A., Dai, J.M. and Sun, Y.P. (2013) Enhanced Microwave Absorption Properties of Carbonyl Iron/Fe₃O₄ Composites Synthesized by a Simple Hydrothermal Method. *Journal of Alloys and Compounds*, **561**, 65-70. <http://dx.doi.org/10.1016/j.jallcom.2013.02.007>

- [15] Ramos Guivar, J.A., Bustamante, A., Flores, J., Mejía Santillan, M., Osorio, A.M., Martínez, A.I., De Los Santos Valldares, L. and Barnes, C.H. (2014) Mössbauer Study of Intermediate Superparamagnetic Relaxation of Maghemite (γ -Fe₂O₃) Nanoparticles. *Hyperfine Interactions*, **224**, 89-97. <http://dx.doi.org/10.1007/s10751-013-0864-z>
- [16] Jiang, W.J., Pelaez, M., Dionysiou, D.D., Entezari, M.H., Tsoutsoud, D. and O'Shea, K. (2013) Chromium (VI) Removal by Maghemite Nanoparticles. *Chemical Engineering Journal*, **222**, 527-533. <http://dx.doi.org/10.1016/j.cej.2013.02.049>
- [17] Papaefthymou, G.C., Devlin, E., Simopoulos, A., Yi, D.K., Riduan, S.N., Lee, S.S. and Ying, J.Y. (2009) Interparticle Interactions in Magnetic Core/Shell Nanoarchitectures. *Physical Review B*, **80**, Article ID: 024406.
- [18] Hai, H.T., Kura, H., Takahashi, M. and Ogawa, T. (2010) Facile Synthesis of Fe₃O₄ Nanoparticles by Reduction Phase Transformation from γ -Fe₂O₃ Nanoparticles in Organic Solvent. *Journal of Colloid and Interface Science*, **341**, 194-199. <http://dx.doi.org/10.1016/j.jcis.2009.09.041>
- [19] Chen, D.X., Sanchez, A., Taboada, E., Roig, A., Sun, N. and Gu, H.C. (2009) Size Determination of Superparamagnetic Nanoparticles from Magnetization Curve. *Journal of Applied Physics*, **105**, Article ID: 083924. <http://dx.doi.org/10.1063/1.3117512>
- [20] Hyeon, T., Lee, S.S., Park, J., Chung, Y. and Na, H.B. (2001) Synthesis of Highly Crystalline and Monodisperse Maghemite Nanocrystallites without a Size-Selection Process. *Journal of the American Chemical Society*, **123**, 12798-12801. <http://dx.doi.org/10.1021/ja016812s>
- [21] Abbas, M., Takahashi, M. and Kim, C. (2013) Facile Sonochemical Synthesis of High-Moment Magnetite (Fe₃O₄) Nanocube. *Journal of Nanoparticle Research*, **15**, 1354. <http://dx.doi.org/10.1007/s11051-012-1354-y>
- [22] Lu, H.M., Zheng, W.T. and Jiang, Q. (2007) Saturation Magnetization of Ferromagnetic and Ferromagnetic Nanocrystals at Room Temperature. *Journal of Physics D: Applied Physics*, **40**, 320-325. <http://dx.doi.org/10.1088/0022-3727/40/2/006>
- [23] Cornell, R.M. and Schwertmann, U. (2003) *The Iron Oxides: Structure, Properties, Reactions, Occurrences and Uses*. Wiley VCH, Hoboken. <http://dx.doi.org/10.1002/3527602097>
- [24] Coaquira, J.A.H., Vaccari, C.B., Tedesco, A.C. and Morais, P.C. (2009) Magnetic Investigation of CoFe₂O₄ Nanoparticles Supported in Biocompatible Polymeric Microsphere. *IEEE Transactions on Magnetics*, **45**, 405-40629. <http://dx.doi.org/10.1109/TMAG.2009.2026291>
- [25] Morup, S., Bodker, F., Hendriksen, P.V. and Linderroth, S. (1995) Spin-Glass-Like Ordering of the Magnetic Moments of Interacting Nanosized Maghemite Particles. *Physical Review B*, **52**, 287.
- [26] Tronc, E., Fiorani, D., Nogues, M., Testa, A.M., Lucari, F., D'Orazio, F., Greneche, J.M., Wernsdorfer, W., Galvez, N., Chanéac, C., Maily, D. and Jolivet, J.P. (2003) Surface Effects in Noninteracting and Interacting γ -Fe₂O₃ Nanoparticles. *Journal of Magnetism and Magnetic Materials*, **262**, 6-14. [http://dx.doi.org/10.1016/S0304-8853\(03\)00011-8](http://dx.doi.org/10.1016/S0304-8853(03)00011-8)
- [27] Carpenter, E.E. (2001) Iron Nanoparticles as Potential Magnetic Carriers. *Journal of Magnetism and Magnetic Materials*, **225**, 17-20.

Scientific Research Publishing (SCIRP) is one of the largest Open Access journal publishers. It is currently publishing more than 200 open access, online, peer-reviewed journals covering a wide range of academic disciplines. SCIRP serves the worldwide academic communities and contributes to the progress and application of science with its publication.

Other selected journals from SCIRP are listed as below. Submit your manuscript to us via either submit@scirp.org or [Online Submission Portal](#).

